Pergamon

Int. J. Heat Mass Transfer. Vol. 38, No. 7, pp. 1225–1236, 1995

0017–9310/95 $9.50+0.00

0017–9310(94)00242–8

Turbulent heat transfer in a serpentine channel with a series of right-angle turns

J. M. CHOI† and N. K. ANAND‡

Department of Mechanical Engineering, Texas A&M University, College Station, TX 77843, U.S.A.

(*Received* 7 *February* 1994 *and in final form* 22 *July* 1994)

Abstract—Turbulent heat transfer in a two-dimensional serpentine channel with a series of right-angle turns was numerically studied. The standard k–ε model was incorporated for turbulence closure. The governing equations were solved by the finite volume technique. The numerical model was validated by comparing the predicted Nusselt number distributions with the experimental data obtained by the naphthalene sublimation technique. The comparison of numerically predicted values of average Nusselt number with the experimental data was fair with a maximum error of 17.4%. Calculations were made for a wide range of geometric and flow parameters (Re = 15 000–60 000). Consideration was given to high (Pr = 7.0) and low (Pr = 0.7) Prandtl number fluids. Correlations for average Nusselt number and frictional factors were developed using the method of least squares. Heat transfer was found to be more sensitive to the Reynolds number in a high Prandtl number fluid than for a low Prandtl number fluid. The maximum values of heat transfer enhancement and friction factor were found in channels with a relatively small undulation height (1–1.5 times the channel width).

INTRODUCTION

Several techniques have been developed to augment single phase convective heat transfer in channels. One technique is to use a serpentine channel [Fig. 1(a)] that increases the heat transfer area in a given volume and enhances the heat transfer due to flow mixing and periodic interruption of thermal boundary layers. This technique has been applied to compact heat exchangers and thermal regenerators. In addition, labyrinth seals in turbomachines resemble the present geometry.

Industrial applications deploy many geometrically identical modules. In such geometries, the flow and temperature fields repeat periodically from module to module after a certain entrance length. Consequently, since most modules are expected to be in the periodically fully developed region, the entrance effects are considered relatively small. It is possible to save computational effort by analyzing flow and heat transfer characteristics in one periodically fully developed module rather than in a whole channel [Fig. 1(b)]. In addition, values of heat transfer coefficient and fluid friction factor in the periodically fully developed flow region are the lower bound forming a basis for design.

The flow in a periodically bent channel shows complex flow patterns such as separation, recirculation, reattachment, deflection, and impingement. The heat transfer augmentation can be explained in terms of these flow mechanisms. The heat transfer enhancement is accompanied by an increase in pressure drop. A heat transfer enhancement technique that requires an unjustifiably high pressure drop is normally not preferred in practice. However, a high pressure drop is beneficial and desired in labyrinth seals.

The detailed heat transfer distribution will help an engineer understand the heat transfer characteristics in a serpentine channel. An experimentally validated numerical model is an economic tool for design and optimization of serpentine channels.

The first numerical solution procedure for periodically fully developed flow and heat transfer was shown by Patankar *et al.* [1]. Faas and McEligot [2] numerically studied flow in a periodically corrugated wall channel in the laminar flow regime. Amano [3] and Amano *et al.* [4] numerically studied heat transfer and fluid flow in similar geometries in laminar and turbulent regimes and compared the results with experimental data. However, the flows in these channels did not have a 180° direction change as shown in Fig. 1(a), but maintained the same flow direction after two right-angle turns. Chang *et al.* [5], Choi *et al.* [6] and Iacovides *et al.* [7] numerically investigated curved U-bends of square cross-section in a turbulent flow regime. Conjugate effects in a channel with one 180° sharp turn was numerically studied by Choi *et al.* [8]. The identical channel in the present study was numerically investigated in a laminar flow regime by Choi and Anand [9].

The objectives of the present investigation are to establish optimum geometrical and flow parameters for turbulent heat transfer in serpentine channels under periodically fully developed conditions. Parametric studies were carried out using an experi-

† Presently with Korean Aerospace Research Institute, Taejon, Korea.

‡ Author to whom correspondence should be addressed.

NOMENCLATURE

C_p specific heat of a working fluid at constant pressure
D_H hydraulic diameter, $2H$
f_o Fanning friction factor for a straight channel
$\bar{f}$ average Fanning friction factor, equation (4)
G amplitude of the channel, Fig. 1(b)
GR G ratio, G/H
H channel width, Fig. 1(b)
h convective heat transfer coefficient, equation (10)
$\bar{h}_{LM}$ average convective heat transfer coefficient by log-mean temperature difference, equation (14)
K thermal conductivity of a working fluid
L half module length, Fig. 1(b)
L_{fl} flow passage length of half module, $AIJK$ in Fig. 1(b)
$\dot{m}$ total mass flow rate, $\rho\bar{u}H$
Nu Nusselt number, hD_H/K
$\overline{Nu}_{int}$ regionally averaged Nusselt number by an area integration in Fig. 2
Nu_o Nusselt number in a straight channel
$\overline{Nu}$ total average Nusselt number
$\overline{Nu}_l$ average Nusselt number for the lower wall
$\overline{Nu}_u$ average Nusselt number for the upper wall
$(\overline{Nu})_{LM}$ average Nusselt number by log-mean temperature difference
p pressure
$\hat{p}$ local variation of pressure, equation (1)
Pr Prandtl number, $C_p\mu/K$
Q_{tot} total heat transferred through the wall
q''_w heat flux at the wall to a working fluid
R distance between inner corners of the channel, Fig. 1(b)
Re Reynolds number, $\rho\bar{u}D_H/\mu$
RR R ratio (R/H)
s coordinate along the wall surface, Figs. 2 and 3
S_{up} upper wall surface area [$AIJK$ in Fig. 1(b)]
T temperature
T_b bulk temperature, equations (7) and (8)
T_w wall temperature
u, v velocities in x- and y-directions
$\bar{u}$ average u velocity in the channel
x, y horizontal and vertical coordinates to the channel.

Greek symbols

β constant representing the overall pressure gradient, equation (1)
$(\Delta T)_{LM}$ log-mean temperature difference, equation (15)
μ dynamic viscosity
ρ density.

Subscripts

b bulk
fl flow passage
l lower wall
LM log-mean difference
o straight channel
u upper wall
w wall.

mentally validated numerical model. The heat transfer enhancement and the friction factor increase were numerically predicted in various geometries. A two-dimensional steady turbulent flow was considered for the current study.

NUMERICAL MODEL AND SOLUTION PROCEDURE

Figure 1(b) shows one module ($ABEF$) of the geometry considered in computation. To save computational effort Choi and Anand [9] used only a half module such as ($ABCD$). They observed that the flows in the half modules $ABCD$ and $DCEF$ hold inverted symmetric relations. Kelkar and Patankar [10] explained in detail this inverted symmetry boundary condition. Since the half module for the experimental study was defined differently [11, 12], one complete module was considered for easier comparison with the experimental data. However, all parametric numerical runs were made with one half modules. Two geometric parameters characterize the present serpentine channel. One is the ratio (GR) of the amplitude G to the channel width H. The other is the ratio (RR) of the distance between inner corners R and the channel width H [Fig. 1(b)]. For example, the channel with a large value of GR corresponds to the high amplitude channel while the channel with a large value of RR corresponds to the long wave length channel. A low value of GR ($GR = 0.5$) corresponds to a straight channel with staggered blockages as shown in Fig. 1(c), and a very low value of RR ($RR = 0.1$) corresponds to a straight channel with staggered fins as shown in Fig. 1(d).

The standard k–ε model (Launder and Spalding [13]) which is a typical two-equation turbulence model was adopted in this study. There are two versions of the k–ε turbulence model, viz. the standard model

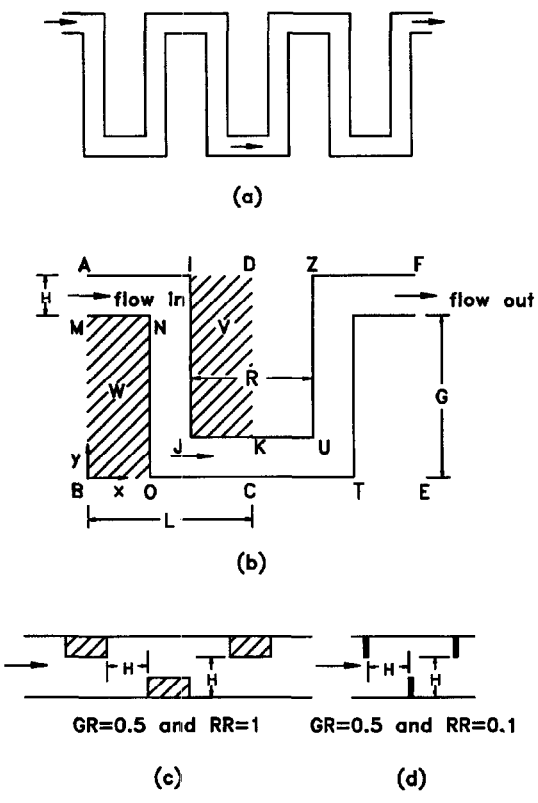

Fig. 1. Serpentine channel models.

with the wall-function method and the low-Reynolds-number version. Ciofalo and Collins [14] reported that the low-Reynolds-number model needs an extremely fine mesh near the wall and, moreover, the heat transfer prediction is not reliable in the re-attachment region. Therefore, the standard k–ε turbulence model with the wall-function method was chosen to study the flow and the heat transfer in this investigation.

Patankar *et al.* [1] explained that the pressure p can be decomposed into two terms for the periodically fully developed flow conditions:

$$p(x,y) = -\beta x + \hat{p}(x,y) \tag{1}$$

where β is a constant representing the total pressure gradient applied to the flow, and $\hat{p}(x,y)$ is the local variation of pressure. The governing equations for the periodically fully developed flow and temperature and their periodic relations in a half module can be written as

$$\frac{\partial}{\partial x}(\rho u\phi)+\frac{\partial}{\partial y}(\rho v\phi)=\frac{\partial}{\partial x}\left(\Gamma_\phi\frac{\partial\phi}{\partial x}\right)+\frac{\partial}{\partial y}\left(\Gamma_\phi\frac{\partial\phi}{\partial y}\right)+S_\phi. \tag{2}$$

The ϕ represents generalized variables such as u, v, T, k and ε. Γ_ϕ and S_ϕ stand for the appropriate diffusion coefficient and the source term, respectively. The details are tabulated in Table 1. The Reynolds number (Re) was defined as

$$\rho\bar{u}D_H/\mu \tag{3}$$

where $\bar{u}$ is the average u velocity at the inlet or exit of the module, and D_H is the hydraulic diameter ($2H$).

The average Fanning friction factor was defined as

$$\bar{f}=\frac{0.25\beta D_H}{0.5\rho\bar{u}^2}\frac{L}{L_{fl}}=\frac{\beta D_H}{2\rho\bar{u}^2}\frac{L}{L_{fl}} \tag{4}$$

where L_{fl} is the flow passage length along the wall in a half module [$AIJK$ in Fig. 1(b)]. L/L_{fl} may be considered a conversion factor by which it is possible to compare the friction factor/pressure drop in a serpentine channel module with one in a straight channel with the same flow passage length under the fully developed condition.

Two common thermal boundary conditions, those of uniform heat flux and uniform wall temperature boundary conditions were considered in the numerical predictions. Patankar *et al.* [1] divided the real temperature in the uniform heat flux boundary condition, into two components. This is similar to what was done in the flow field. However, in this study, T is the real temperature in both cases.

Uniform heat flux boundary condition

Using the periodic and the inverted symmetric nature of the temperature field in the half module, the temperatures at the left and right boundaries have the following relation:

$$T(0,y) = T(L,H+G-y)-\frac{Q_{tot}}{\dot{m}C_p} \tag{5}$$

where $Q_{tot} = q''_w S_{tot}$ and $\dot{m} = \rho\bar{u}H$. The q''_w is the heat flux from the wall to the fluid and is constant in the uniform heat flux boundary condition. The $\dot{m}$ is the total mass flow rate through the module. The S_{tot} indicates total surface area which transfers the constant heat flux q''_w into a working fluid. It should be noticed in equation (5) that the temperatures are not specified on the boundaries but their periodic relation is indicated. By this reason only temperature differences are meaningful.

Uniform wall temperature boundary condition

In the thermally periodically fully developed region, the thermal field which is defined by $(T-T_w)/(T_b-T_w)$ repeats identically from module to module, where T_w and T_b represent the wall temperature and the bulk temperature, respectively. The left and right boundaries have the following relation:

$$\frac{T(0,y)-T_w}{T_b(0)-T_w}=\frac{T(L,H+G-y)-T_w}{T_b(L)-T_w} \tag{6}$$

where the inverted symmetry boundary condition is applied. In addition, $T_b(0)$ can be given any arbitrary value that is different from T_w. Kelkar and Patankar

Table 1. Summary of governing equations

Equation	ϕ	Γ_ϕ	S_ϕ
Continuity	1	0	0
x momentum	u	μ_{eff}	$\beta-\partial\hat{p}/\partial x+S_u$
y momentum	v	μ_{eff}	$-\partial\hat{p}/\partial y+S_v$
Thermal energy	T	$\mu/Pr+\mu_t/Pr_t$	0
Turbulence energy	k	$\mu+\mu_t/\sigma_k$	$P_k-\rho\varepsilon$
Dissipation rate	ε	$\mu+\mu_t/\sigma_\varepsilon$	$(C_1P_k\varepsilon-C_2\rho\varepsilon^2)/k$

where

$$\mu_{\text{eff}}=\mu+\mu_t,\quad \mu_t=C_\mu\rho k^2/\varepsilon$$

$$S_u=\frac{\partial}{\partial x}\left(\mu_{\text{eff}}\frac{\partial u}{\partial x}\right)+\frac{\partial}{\partial y}\left(\mu_{\text{eff}}\frac{\partial v}{\partial x}\right)$$

$$S_v=\frac{\partial}{\partial x}\left(\mu_{\text{eff}}\frac{\partial u}{\partial y}\right)+\frac{\partial}{\partial y}\left(\mu_{\text{eff}}\frac{\partial v}{\partial y}\right)$$

$$p_k=\mu_t\left[\left(\frac{\partial u}{\partial y}+\frac{\partial v}{\partial x}\right)^2+2\left(\frac{\partial u}{\partial x}\right)^2+2\left(\frac{\partial v}{\partial y}\right)^2\right]$$

$$C_\mu=0.09,\quad C_1=1.44,\quad C_2=1.92,\quad \sigma_k=1.0,$$

$$\sigma_\varepsilon=\frac{k^2}{(C_2-C_1)C_\mu^{1/2}},\quad \text{and}\quad Pr_t=0.9.$$

[10] described the computational details. The bulk temperature (T_b) is defined as

$$T_b(x)=\int|u|T\,dy\Big/\int|u|\,dy \tag{7}$$

on AI, JK, MN and OC surfaces, and

$$T_b(x)=\int|v|T\,dy\Big/\int|v|\,dy \tag{8}$$

on IJ and NO surfaces in Fig. 1(b). The integrations are carried out over the cross-section of the channel. The absolute values of the velocities are used to account for recirculating flows. The bulk temperature definition is also applicable in the uniform heat flux boundary condition.

Nusselt number

The local Nusselt number is defined as

$$Nu=\frac{hD_H}{K} \tag{9}$$

where K is the thermal conductivity of a working fluid and h is defined as

$$h=\frac{q''_w}{(T_w-T_b)}. \tag{10}$$

By substituting equation (10) into equation (9), Nu can be expressed as follows:

$$Nu=\frac{q''_wD_H}{K(T_w-T_b)}. \tag{11}$$

For the uniform heat flux boundary condition q''_w is constant while it becomes a function of the location and a part of solution for the uniform temperature boundary condition. The wall temperature T_w is a constant value for the uniform wall temperature boundary condition while it becomes a function of the location and a part of solution for the uniform heat flux boundary condition.

The average Nusselt number for the upper wall ($\overline{Nu}_u$) was defined as

$$\overline{Nu}_u=\frac{1}{S_{up}}\int Nu\,dS \tag{12}$$

where S_{up} is the upper wall surface area [$AIJK$ in Fig. 1(b)]. In the same way, the average Nusselt number for the lower wall ($\overline{Nu}_l$) was defined with the lower wall surface area [$MNOC$ in Fig. 1(b)]. Since the upper wall has the same surface area as the lower wall, the total average Nusselt number ($\overline{Nu}$) is the arithmetic mean of the two Nusselt numbers.

For the uniform wall temperature boundary condition, one more definition of the average Nusselt number is commonly used. The average Nusselt number based on the log-mean temperature difference is defined as

$$(\overline{Nu})_{LM}=\frac{\bar{h}_{LM}D_H}{K}. \tag{13}$$

The average convective heat transfer coefficient ($\bar{h}_{LM}$) based on the log-mean temperature difference in equation (13) is defined as

$$\bar{h}_{LM}=\frac{Q_{tot}/S_{tot}}{(\Delta T)_{LM}} \tag{14}$$

where S_{tot} is the total surface area [$AIJK$ and $MNOC$ in Fig. 1(b)]. The log-mean temperature difference $(\Delta T)_{LM}$ in equation (13) is defined as

$$(\Delta T)_{LM}=\frac{(T_w-T_b(0))-(T_w-T_b(L))}{\ln\left((T_w-T_b(0))/(T_w-T_b(L))\right)}. \tag{15}$$

The Q_{tot} in equation (14) was defined as

$$Q_{tot} = \int q''_w \, dS \tag{16}$$

where the integration is carried out over the top and bottom surfaces [*AIJK* and *MNOC* in Fig. 1(b)] and q''_w is the heat flux on the wall. The difference between the total average Nusselt number ($\overline{Nu}$) and the average Nusselt number based on log-mean temperature difference ($\overline{Nu}$)$_{LM}$ was negligible in the present work [12].

Independent parameters

The Prandtl number (*Pr*), the channel geometry, and the Reynolds number (*Re*) were the independent parameters that influenced heat transfer characteristics in the present channels. Air and water at room temperature were considered as working fluids and their Prandtl numbers are 0.7 and 7.0, respectively. Two geometric parameters (*GR* and *RR*) were discussed earlier. The range of Reynolds numbers considered in this study was $Re = 18\,460$–$60\,000$.

Computational details

A **FORTRAN** program that utilizes the finite volume technique described by Patankar [15] was developed to solve the governing equations. The pressure and velocity fields were linked by the Semi-Implicit Method for Pressure-Linked Equations Revised (SIMPLER) algorithm. The interaction of convection and diffusion terms was handled by the power law scheme. The resulting set of discretization equations was solved by a line-by-line technique which uses the tri-diagonal matrix algorithm and the Gauss–Siedel iterative method.

Convergence criteria

The convergence for the velocity field was declared when the total mass residue was less than 1×10^{-5} times the total mass and the relative error between two successive β values was less than 1×10^{-5}. The convergence for the temperature field was declared when the sum of the discretization equations residues was less than 1×10^{-10} times the total heat transfer rate across the channel walls. It took approximately 75 min of **CPU** time on the **Cray Y-MP2/216** supercomputer to meet these criteria for a reference run (128×80 mesh).

Grid independence

One complete module with uniform wall temperature was considered for the grid independence study. The grid independence was declared between 128×80 and 160×100 uniformly spaced meshes at $GR = 1.5$, $RR = 1$ and $Re = 100\,000$. The maximum velocity and temperature differences between the two meshes at the module inlet were 2.25 and 0.46%, respectively. The maximum differences occurred in the recirculation zone while the differences in other regions were negligible [12]. The differences in pressure drop and average Nusselt number based on the log-mean temperature difference were 1.46 and 0.43%, respectively. Hence, the 128×80 mesh was selected as a reference mesh size.

Table 2. Comparison of $(\overline{Nu})_{LM}$ in the periodically fully developed condition module between the experiment and computation

Re	Experiment	Computation	Relative error [%]
18 460	189.6 ± 15.0	161.1	15.0
32 940	316.5 ± 25.0	261.3	17.4

EXPERIMENTAL VALIDATION

Since the validation and limitations of the present numerical model are available in other references [11, 12] along with the experimental results, only major points are presented here. For the purpose of validation of the numerical model, the average Nusselt numbers in the periodically fully developed condition were compared with the ones from the naphthalene sublimation experiments (Table 2). The numerical results at both low ($Re = 18\,460$) and high ($Re = 32\,940$) Reynolds numbers underpredict the experimental results. The maximum relative error is 17.4%. The relative error is defined by normalizing the difference between the experimental and numerical values with respect to the experimental value.

Figure 2 shows a comparison of local Nusselt number distributions between the experimental data and numerical predictions in the periodically fully developed region. The numerical model predicts the local Nusselt number distribution well on the plate (a, b in Fig. 2) and top (c, d) surfaces while the predictions on the front (b, c) and back (d, e) are not satisfactory. The discrepancy between the experimental data and numerical prediction on the front surface can be explained from the fact that the standard k–ε model underpredicts the area of the recirculation zone. For the discrepancy on the back surface, it was speculated that the k–ε model cannot predict the high turbulence and/or a possible large scale motion (e.g. strong small vortex) in the shear layer and recirculation zones [11, 12].

Tables 3 and 4 show the comparison of the regionally averaged Nusselt numbers by an integration of area in Fig. 2 ($\overline{Nu}_{int}$) at $Re = 18\,460$ and 32 940, respectively. The integration was done by using the trapezoidal rule for both curves (experiment and computation). The relative error was defined by normalizing the difference between the experimental and numerical values with respect to the experimental value. The comparison is quite good at the top surface (as small as 7.8% error) but not satisfactory at the back surface (up to 34.0% error).

In summary, the numerically predicted average and regionally averaged Nusselt numbers agree well with the experimental data. However, the agreement of

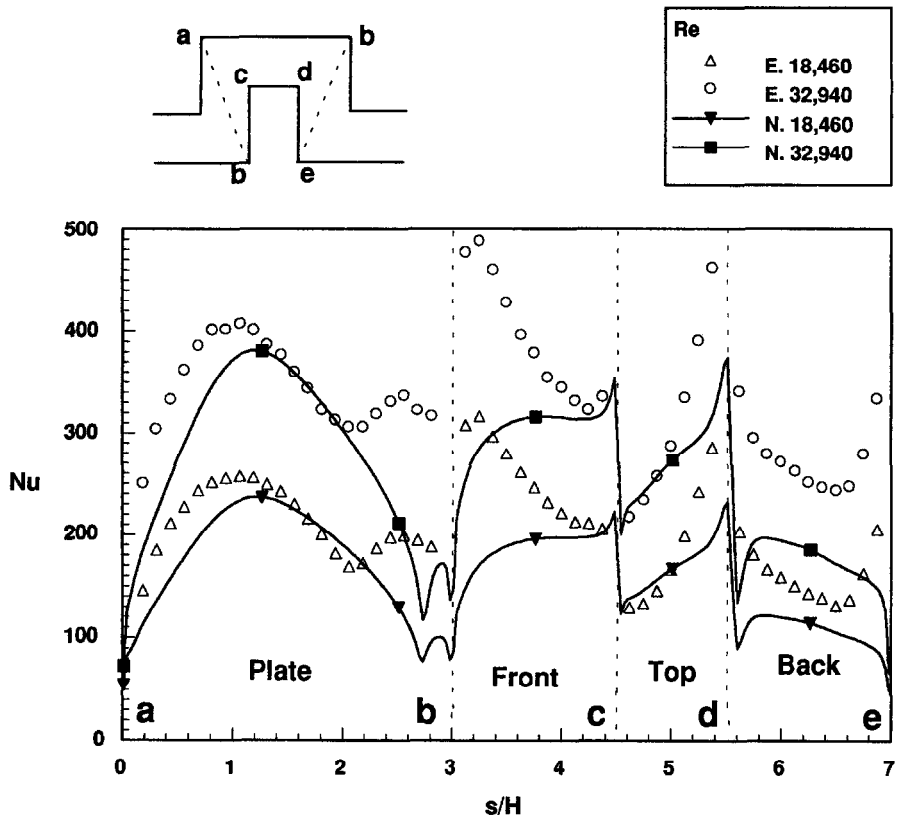

Fig. 2. Comparison of local Nusselt number distributions between experiments and numerical predictions at $Pr = 0.7$ ($GR = 1.5$ and $RR = 1$): (E) experiment, (N) numerical prediction.

Table 3. Comparison of $\overline{Nu}_{int}$ between the experiment and the computation at $Re = 18460$

	$\overline{Nu}_{int}$ Experiment	$\overline{Nu}_{int}$ Computation	Relative error [%]
Plate	213.7	183.2	14.3
Front	253.3	189.4	25.2
Top	182.2	167.9	7.8
Back	157.2	110.0	30.0

predicted local Nusselt number distribution with the experimental data is less than satisfactory. Nevertheless, the focus of this work is to develop correlations for average Nusselt numbers for serpentine channels under periodically fully developed flow conditions. Accordingly, this degree of agreement can be considered fair.

Table 4. Comparison of $\overline{Nu}_{int}$ between the experiment and the computation at $Re = 32940$

	$\overline{Nu}_{int}$ Experiment	$\overline{Nu}_{int}$ Computation	Relative error [%]
Plate	347.7	295.6	15.0
Front	391.4	307.1	21.5
Top	307.2	269.7	12.2
Back	270.9	178.9	34.0

RESULTS AND DISCUSSION

Figure 3 shows the typical overview of the heat transfer enhancement in the serpentine channels. For illustration, the heat transfer enhancement ratio ($\overline{Nu}/Nu_0$) is defined so that the average Nusselt number for the considered geometry in the periodically fully developed condition is normalized with respect to the Nusselt number for a straight channel in the fully developed condition. The average Nusselt number (Nu_0) in a straight channel was calculated using Dittus Boelter equation [16].

The heat transfer enhancement trends are almost the same regardless of the Reynolds and Prandtl numbers. The heat transfer enhancement ratio has a peak with respect to GR while it monotonically decreases with RR. The maximum enhancement ratio is found in the channel with $GR = 1$ and the smallest value of RR ($RR = 0.25$ in the present study) for all cases. The minimum enhancement ratio is found in the channel with the smallest value of GR ($GR = 0.5$ in the present study) and largest value of RR ($RR = 2$ in the present study). Since the channel with $GR = 0$ corresponds to a straight channel, its heat transfer enhancement ratio becomes unity. It is obvious that the minimum enhancement ratio is found in the channel with the smallest value of GR (close to zero).

Figure 4 shows that heat transfer is more sensitive to the Reynolds number in the high Prandtl number

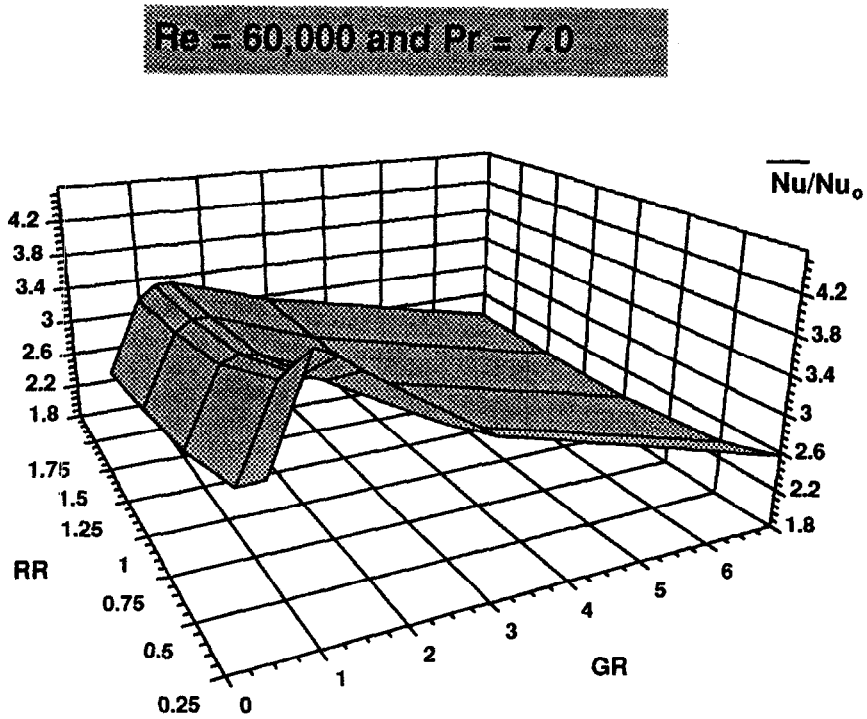

Fig. 3. Overview of heat transfer enhancement at $Re = 60\,000$ and $Pr = 7.0$ (maximum enhancement ratio: 4.41 at $GR = 1$ and $RR = 0.25$) (minimum enhancement ratio: 2.28 at $GR = 7$ and $RR = 1.5$).

fluid. The enhancement ratio curve at $Pr = 7.0$ has a steeper slope than the one at $Pr = 0.7$. For this reason, even though the enhancement ratio at $Pr = 7.0$ is lower than the one at $Pr = 0.7$ at the low Reynolds number ($Re = 18\,460$), it outgrows the enhancement ratio at $Pr = 0.7$ as Re increases. This phenomenon is also seen in the laminar flow regime (Choi and Anand [9]). However, there is a slight difference between the heat transfer enhancement in the laminar flow regime and the turbulent flow regime. In the laminar flow regime, the Nusselt number in a straight channel or pipe is constant regardless of Re and Pr in the fully developed condition. Consequently, the small values of slope of the enhancement ratio curve causes very little increase in the absolute value of the Nusselt number with Re. However, in the turbulent flow regime, since the Nusselt number in a straight channel or pipe is a function of Re and Pr, the absolute value of the average Nusselt number in the serpentine channel continues to increase with Re even though the slope of the enhancement ratio is small. The absolute values of the average Nusselt numbers in the other channels are available in Choi [12]. In addition, the effect of thermal boundary condition on local Nusselt number distribution was examined. As expected for turbulent flow the heating condition (uniform wall temperature/uniform heat flux) had no impact on the local Nusselt number. Details are reported elsewhere [12].

Figure 5 shows that the maximum enhancement ratio is found in the channel with a higher value of GR as RR increases. The maximum enhancement is found in the channel with $GR = 1$ when RR has the smallest value ($RR = 0.25$) and in the channel with $GR = 1.5$ when RR has the highest value ($RR = 2$). Graphically, the curve for $GR = 1$ is positioned below that for $GR = 1.5$. The enhancement ratio in the channel with the high value of GR ($GR = 7$) does not change much with RR.

To examine which wall is more effective from a heat transfer point of view, the average Nusselt number ($\overline{Nu}_u$) for the upper wall is normalized with respect to the average Nusselt number ($\overline{Nu}_l$) for the lower wall in Fig. 6. The straight line parallel to the abscissa means that the average Nusselt number ratio is unity and both walls have the same heat transfer coefficients. Normally the upper wall is more effective in heat transfer than the lower wall even though the average Nusselt number ratio becomes smaller and approaches unity as RR increases [Fig. 6(a)]. However, as can be seen in Fig. 6(b), the lower wall becomes more effective than the upper wall in some channels. This phenomenon occurs in channels with $GR = 1$–2 when $RR > 1.5$.

Based on numerical simulation, the absolute value of the friction factor was found to be a weak function of the Reynolds number in the range considered ($Re = 18\,460$–$60\,000$). This fact agrees with the experimental result [12]. However, since the friction factor in a straight channel is a function of the Reynolds

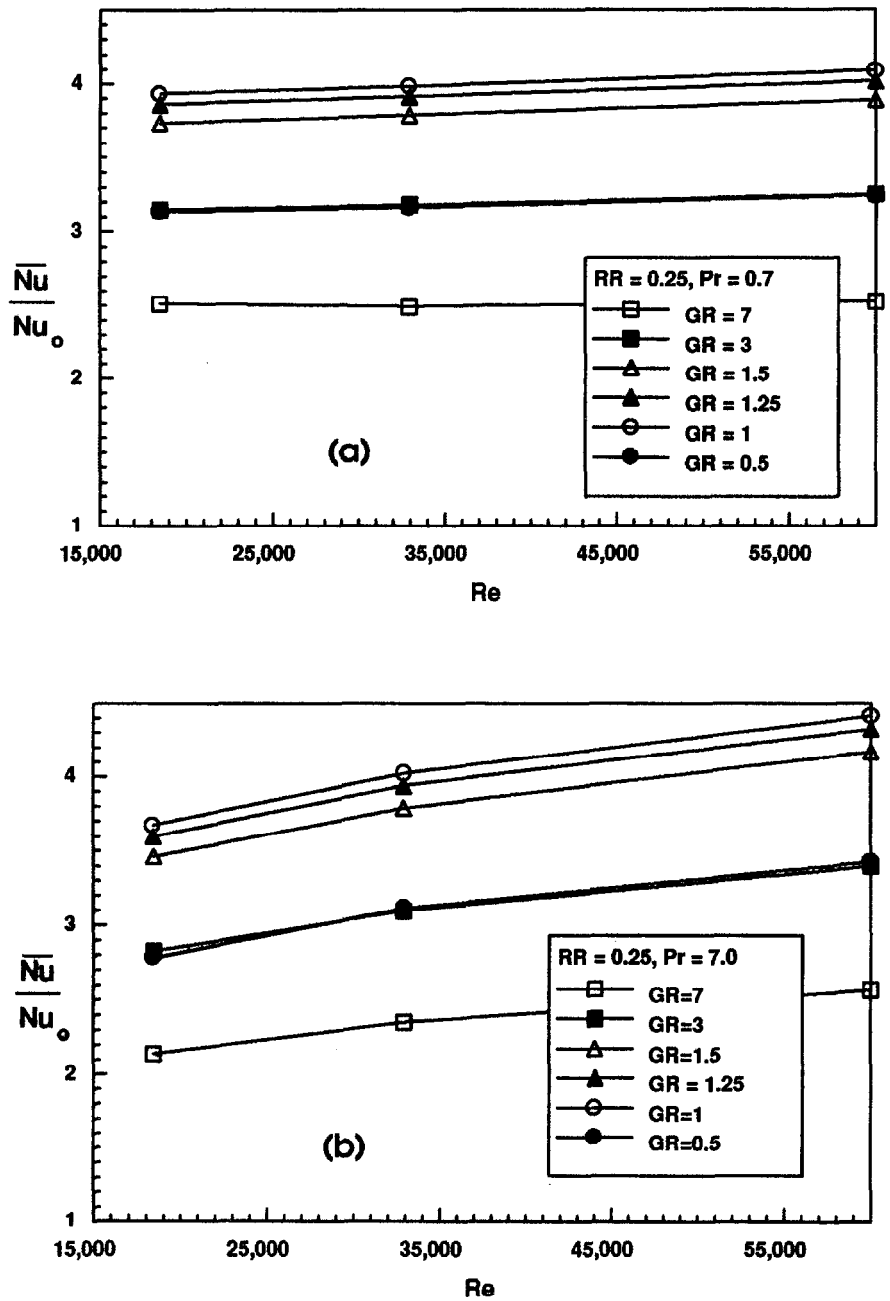

Fig. 4. Variation of heat transfer enhancement ratio with Re at $RR = 0.25$: (a) $Pr = 0.7$, (b) $Pr = 7.0$.

number [17], the ratio of the friction factor in the considered channel to that of a straight channel becomes a function of the Reynolds number.

As seen in Fig. 3 and ref. [12], the distributions of the average Nusselt number ratio and the friction factor ratio have non-monotonic variation with GR while they monotonically decrease with RR. For this reason it is difficult to develop a unique correlation to cover all the geometrical parameters (GR and RR). Alternatively, one correlation is suggested for each GR value.

Both the average Nusselt number and friction factor ratios are correlated with the Reynolds number and the geometrical parameter RR by

$$\overline{Nu}/Nu_o \quad \text{or} \quad \bar{f}/f_o = c\,Re^a\,RR^b \tag{17}$$

where a, b, and c are constant coefficients for a specified GR. The numerical values of these coefficients are listed in Tables 5–7. It should be noticed that the value for f_o is from the Beavers *et al.* correlation [17].

The abbreviation SEE in Tables 5–7 stands for the standard error of estimate. It is a measure of the scatter of real data about the regression line and its properties are analogous to those of the standard devi-

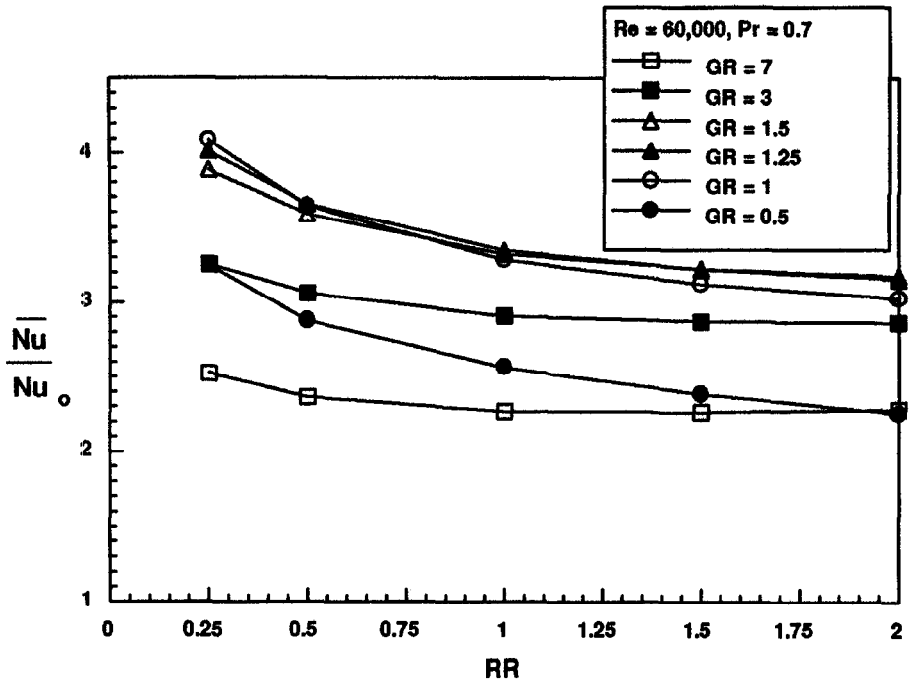

Fig. 5. Variation of heat transfer enhancement ratio with RR at $Re = 60\,000$ and $Pr = 0.7$.

ation. Usually a small value of SEE indicates that most of the data are clustered near the regression line or that the regression line predicts the real data well. The standard error of estimate is an absolute and not a relative value. SEE will be big if the data are very large numbers although the correlation predicts the data very accurately. For this reason, the mean value in each series of channels (each specified GR) is included in the table. For example, even though the SEE (= 3.3355) of the friction factor correlation at $GR = 1$ is larger than the SEE (= 1.2123) at $GR = 7$ in Table 7, the friction factor correlation at $GR = 1$ is more accurate than the one at $GR = 7$ since the former has the much larger mean value than the latter.

The coefficient 'a' in equation (17) is a barometer indicating how much the Reynolds number change influences the average Nusselt number ratio or the friction factor ratio, and the coefficient 'b' in equation (17) is a counterpart for the geometrical parameter RR. In both cases, the absolute values are important and the negative sign means that it has an inverse effect. All the coefficients 'a' in Table 6 are higher than the ones in Table 5. This implies that the average Nusselt number ratio is more sensitive to the Reynolds number for high Prandtl number fluid than for low Prandtl number fluid. The coefficients 'b' for lower values of GR are higher than the ones for higher values of GR in Tables 5–7. This implies that the average Nusselt number ratio or the friction factor ratio in the channel with a lower value of GR is more sensitive to the change in RR than in the channel with a higher value of GR. The above facts were shown in Figs. 4 and 5.

CONCLUSIONS

With the experimentally validated numerical model, the heat transfer and flow characteristics of a serpentine channel were investigated and their optimum conditions were numerically explored by the parametric study. The considered ranges of the parameters are $Re = 18\,460$–$60\,000$, $Pr = 0.7$ and 7.0, $GR = 0.5$–7 and $RR = 0.25$–2. The average Nusselt number and friction factor in the serpentine channel were normalized with respect to the ones corresponding to a fully developed condition in straight channels. From the numerical study, the following conclusions are drawn:

(1) Significant heat transfer enhancement is obtained in both low and high Prandtl number fluids. The maximum enhancement ratio is 4.41 and found in the channel with $GR = 1$ and the lowest value of RR ($RR = 0.25$) at $Re = 60\,000$ and $Pr = 7.0$.

(2) Heat transfer is more sensitive to the Reynolds number for high Prandtl number fluid ($Pr = 7.0$) than for low Prandtl number fluid ($Pr = 0.7$). Consequently, the heat transfer enhancement ratio is larger for the high Prandtl number fluid compared to that for the low Prandtl number fluid at high Reynolds number ($Re = 60\,000$). It is the opposite at low Reynolds number ($Re = 18\,460$).

(3) The maximum heat transfer enhancement is found in the channel with $GR = 1$ when RR value is low while it is found in the channel with $GR = 1.5$ when RR value is large. The trends

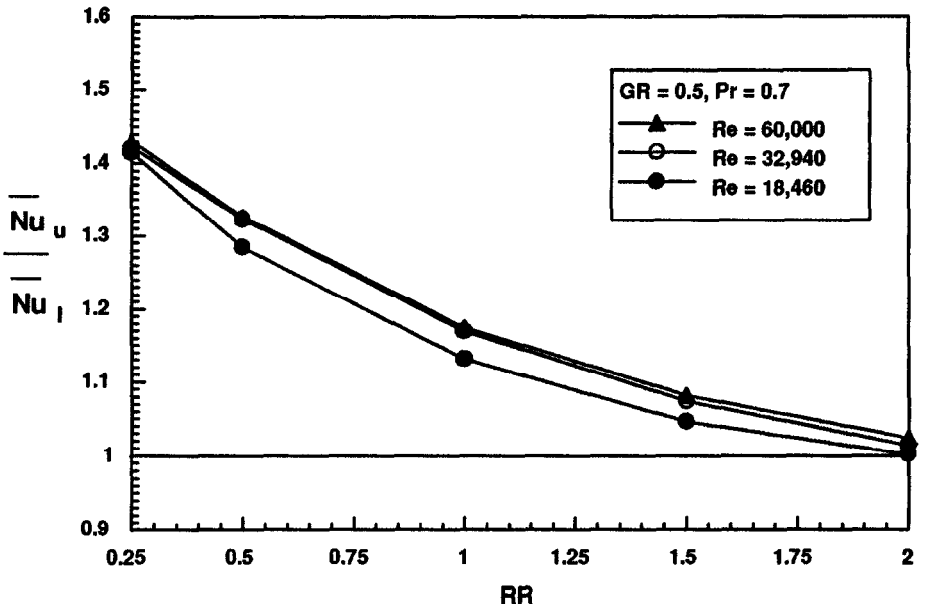

(a) GR = 0.5 and Pr = 0.7

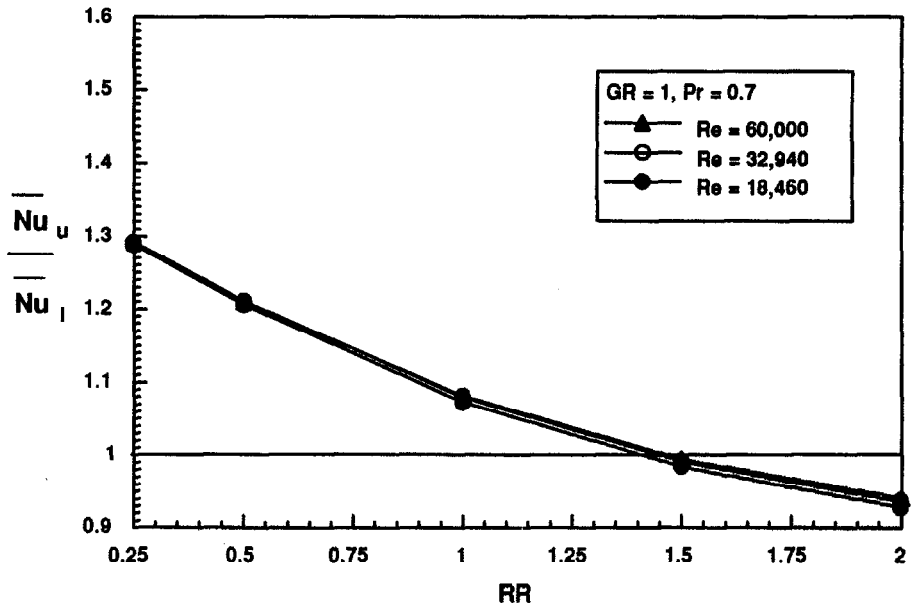

(b) GR = 1 and Pr = 0.7

Fig. 6. Average Nusselt number ratio between upper and lower walls: (a) $GR = 0.5$ and $Pr = 0.7$, (b) $GR = 1$ and $Pr = 0.7$.

of the friction factor ratio [12] is the same as the heat transfer enhancement ratio.

(4) The absolute value of the friction factor in the serpentine channel does not vary much in the range of Reynolds numbers considered but the friction factor ratio increases with Re [12].

(5) The heat transfer enhancement ratio and the friction factor [12] ratio decrease monotonically with an increase in RR while they have non-monotonic variation with respect to GR. For this reason correlation equations were developed for each value of GR.

Table 5. Coefficients of correlation equation (17) for $\overline{Nu}/Nu_o$ at $Pr = 0.7$

GR	c	a	b	Mean	SEE
0.5	2.0266	0.02051	−0.1641	2.6177	0.02547
1	2.2055	0.03678	−0.1471	3.3508	0.03072
1.25	2.2295	0.03767	−0.1196	3.3930	0.03203
1.5	2.2041	0.03820	−0.1005	3.3564	0.03208
3	2.0997	0.03074	−0.0640	2.9321	0.03427
7	2.1546	0.00605	−0.0526	2.3207	0.04049

Table 6. Coefficients of correlation equation (17) for $\overline{Nu}/Nu_o$ at $Pr = 7.0$

GR	c	a	b	Mean	SEE
0.5	0.33494	0.18740	−0.1973	2.4867	0.01527
1	0.52193	0.17289	−0.1687	3.3010	0.03535
1.25	0.55349	0.16949	−0.1356	3.3469	0.03804
1.5	0.56404	0.16692	−0.1151	3.3024	0.03883
3	0.46989	0.17012	−0.0740	2.8155	0.04014
7	0.37286	0.16685	−0.0596	2.1520	0.04459

Table 7. Coefficients of correlation equation (17) for $\bar{f}/f_o$

GR	c	a	b	Mean	SEE
0.5	1.1001	0.32752	−0.6969	44.543	0.7383
1	2.8504	0.30053	−0.5464	80.193	3.3355
1.25	2.6668	0.30801	−0.4400	77.010	3.6381
1.5	2.4189	0.31167	−0.3667	70.280	3.5148
3	1.3756	0.31263	−0.2156	38.166	1.9683
7	0.7223	0.29599	−0.1691	16.615	1.2123

(6) The upper wall is normally more effective from the heat transfer point of view. However, the lower wall transfers heat more effectively for the channel with GR = 1–2 when RR is greater than 1.5.

Acknowledgements—Financial support from the Texas State Energy Research in Application Program (ERAP, contract #32121-70340), the Texas A&M University Center for Energy and Mineral Resources (CEMR, contract #155134) and the NASA Center of Space Power (contract #2500094) is gratefully acknowledged. Supercomputer time and computing facilities were made available from the Texas A&M University Supercomputer Center and Academic Computing Service.

REFERENCES

1. S. V. Patankar, C. H. Liu and E. M. Sparrow, Fully developed flow and heat transfer in ducts having streamwise-periodic variations of cross-sectional area, *ASME J. Heat Transfer* **99**, 180–186 (1977).
2. S. E. Faas and D. M. McEligot, Convective heat transfer for ship propulsion, Report No. 1248–7, Office of Naval Research, Aerospace and Mechanical Engineering Department, University of Arizona (1980).
3. R. S. Amano, A numerical study of laminar and turbulent heat transfer in a periodically corrugated wall channel, *ASME J. Heat Transfer* **107**, 564–569 (1985).
4. R. S. Amano, A. Bagherlee, R. J. Smith and T. G. Niess, Turbulent heat transfer in corrugated-wall channels with and without fins, *ASME J. Heat Transfer* **109**, 62–67 (1987).
5. S. M. Chang, J. A. C. Humphrey and A. Modavi, Turbulent flow in a strongly curved U-bend and downstream tangent of square cross-sections, *Physico-Chemical Hydrodynamics* **4**(3), 243–269 (1983).
6. Y. D. Choi, H. Iacovides and B. E. Launder, Numerical computation of turbulent flow in a square-sectional 180 deg bend, *ASME J. Fluids Engng* **111**, 59–68 (1989).
7. H. Iacovides, B. E. Launder, P. A. Loizou and H. H. Zhao, Turbulent boundary-layer development around a square-sectional U-bend: Measurements and Computation, *ASME J. Fluids Engng* **112**, 409–415 (1990).
8. J. M. Choi, N. K. Anand and W. R. Laster, Conjugate heat transfer in a U-shaped channel with two right angle turns, *Proceedings of the 9th International Heat Transfer Conference*, 8-MC-06, Vol. 3, pp. 297–302. Jerusalem, Israel (1990).
9. J. M. Choi and N. K. Anand, Heat transfer in a serpentine channel with a series of right-angle turns, *Numer. Heat Transfer* **23**, Part A, 189–210 (1993).
10. K. M. Kelkar and S. V. Patankar, Numerical prediction of flow and heat transfer in a parallel plate channel with staggered fins, *ASME J. Heat Transfer* **109**, 25–30 (1987).
11. J. M. Choi, N. K. Anand and S. C. Lau, Turbulent heat transfer measurement and numerical prediction in

a serpentine channel, 1993 Winter Annual Meeting of ASME, New Orleans, LA, 93-WA/HT-51 (1993).
12. J. M. Choi, Heat transfer in a serpentine channel with a series of right-angle turns, Ph.D. Dissertation, Texas A&M University, College Station, TX (1993).
13. B. E. Launder and D. B. Spalding, The numerical computation of turbulent flows, *Comput. Meth. Appl. Mech. Engng* **3,** 269–289 (1974).
14. M. Ciofalo and M. W. Collins, k–ε Predictions of heat transfer in turbulent recirculating flows using an improved wall treatment, *Numer. Heat Transfer* **15,** Part B, 21–47 (1989).
15. S. V. Patankar, *Numerical Heat Transfer and Fluid Flow*. McGraw-Hill, New York (1980).
16. F. W. Dittus and L. M. K. Boelter, *Univ. Calif. Publs Engng* **2,** 443 (1930).
17. G. S. Beavers, E. M. Sparrow and J. R. Lloyd, Low Reynolds number turbulent flow in large aspect ratio rectangular duct, *ASME J. Basic Engng* **93,** 296–299 (1971).